engineering proceedings

MDPI

Proceeding Paper

Bagasse-Based Cellulose Nanocrystal–Magnetic Iron Oxide Nanocomposite for Removal of Chromium (VI) from Aqua Media †

Evans Suter [1,*], Hilary Rutto [1], Tumisangs Seodigeng [1], Lewis Kiambi [1] and Wesley Omwoyo [2]

[1] Clean Technology and Applied Materials Research Group, Department of Chemical Engineering and Metallurgy, Vaal University of Technology, Private Bag X021, Vanderbijlpark 1900, South Africa; hilaryr@vut.ac.za (H.R.); tumisangs@vut.ac.za (T.S.); lewiskiambi1995@gmail.com (L.K.)

[2] Biotechnology and Chemistry Department, Vaal University of Technology, Private Bag X021, Vanderbijlpark 1900, South Africa; wesleyomwoyo16@gmail.com

* Correspondence: 222386568@edu.vut.ac.za; Tel.: +27-681640423

† Presented at the 3rd International Electronic Conference on Processes—Green and Sustainable Process Engineering and Process Systems Engineering (ECP 2024), 29–31 May 2024; Available online: https://sciforum.net/event/ECP2024.

Abstract: This research developed a low-cost nano-bio-adsorbent using sugar cane bagasse-based nanocrystals incorporated with magnetic iron oxide nanoparticles (CNCs-MIONPs). The adsorbent demonstrated excellent Cr(VI) adsorption efficiency at an optimal pH of 2.0, an initial concentration of 0.5 mg/L, and a contact time of 90 min with a shaking rate of 250 rpm, achieving a removal efficiency of 91.78%. The increased surface area, smaller particle size, and the nanocomposite's active sites facilitated chromium species' immobilisation, enhancing chromate ion removal. The adsorption process involved chemisorption, where valence forces such as electron sharing or exchange occur between the adsorbate and sorbent. The modified CNCs-MIONPs showed improved sorption efficiency, suggesting potential applications in water treatment plants, both for domestic and industrial wastewater.

Keywords: bagasse; cellulose nanocrystals; nanocomposite; adsorption; chemisorption; chromate ions

Citation: Suter, E.; Rutto, H.; Seodigeng, T.; Kiambi, L.; Omwoyo, W. Bagasse-Based Cellulose Nanocrystal–Magnetic Iron Oxide Nanocomposite for Removal of Chromium (VI) from Aqua Media. *Eng. Proc.* **2024**, *67*, 5. https://doi.org/10.3390/engproc2024067005

Academic Editor: Isabel Cansado

Published: 11 July 2024

1. Introduction

The growing global concern about the sensible use of natural resources and the environmental impact of technology is prompting the development of more effective pollution remediation technologies [1]. Water pollution is particularly severe among ecological challenges due to its impact on plant, animal, and human life [2–4]. Heavy metal contamination, especially with metals like chromium, poses significant environmental and public health hazards [5]. Hexavalent chromium (Cr^{6+}) is highly toxic and carcinogenic, and its presence in industrial effluents from sectors such as electroplating, leather tanning, and dyeing necessitates stringent control measures. Permissible chromium levels in livestock and irrigation water are below 0.05 mg/L [6,7]. Various methods exist for removing chromium ions from wastewater, including distillation, chlorination, ion exchange resins, membrane filtration, and adsorption [8,9]. However, these methods often face limitations such as high operational costs, low effectiveness at low pollutant concentrations, and practical challenges for large-scale applications. Ion exchange resins, while common, can be easily contaminated by organic matter, reducing their efficacy. Membrane filtration techniques like nano-filtration and reverse osmosis are more effective but require significant maintenance and operational costs due to high-pressure needs [10].

Nanotechnology has driven significant advancements across various fields, including environmental remediation [11]. Nanomaterials, characterised by their nanoscale size (1–100 nm), exhibit unique properties not found in larger molecules [12]. Iron oxide-based

nanomaterials, in particular, have shown promise for environmental applications due to their high surface area, ease of synthesis, biocompatibility, low toxicity, and superparamagnetic properties [13–15]. These nanoparticles can reduce hexavalent chromium to the less toxic trivalent chromium, facilitating the removal of contaminants from water.

Sugar cane bagasse contains various functional groups, such as carboxylic acid, ester, carboxylate, hydroxyl, phenolic, and amino, making it a potential adsorbent for heavy metal ions [16]. The negative (OH^-) surface functions of the cellulose nanocrystals (CNCs) were enhanced by incorporating magnetic iron oxide nanoparticles (MIONPs), which could improve its adsorption capabilities.

In this study, a low-cost adsorbent (CNCs-MIONPs) was developed and used to remove hexavalent chromium from synthetic wastewater. The produced composite and precursor materials were characterised using SEM and FT-IR, as reported in previous work [14,15].

2. Materials and Methods

2.1. Chemicals and Reagents

The cellulose nanocrystals and the nanocomposite materials were obtained from previous work [14,17]. Sulfuric acid, H_2SO_4 (≥99.9%), sodium hydroxide, Diphenyl Carbazide (DPC), acetone (≥99.9%), and Potassium Dichromate ($K_2Cr_2O_7$) were purchased from Sigma-Aldrich, Meck, Johannesburg South Africa. All the chemicals were analytical grade. Throughout the experiment, deionised water was utilised.

2.2. Methods

The nanocomposite was synthesised via the in situ incorporation of magnetic iron oxide onto CNCs. Briefly, 100 mL of deionised water was measured and poured into a three-neck round-bottomed flask with 1.5 g of CNC powder. The three-necked flask was equipped with a magnetic stirrer and a Liebig condenser. The degassing of the deionised water in the three-neck flask was conducted for 15 min by heating at 80 °C for 15 min, followed by bubbling with nitrogen gas for 15 min to establish an inert environment. To the inert water–chemically purified cellulose (WCPC) mixture, 3.1 g of ferric chloride hexahydrate and 2.1 g of ferrous sulphate heptahydrate salts were added under robust mixing for 1 h, after which 25% NH4OH was added dropwise for co-precipitation until the colour turned dark brown, after which the stirring process was prolonged for an hour. The precipitate was allowed to settle and thereafter washed using a deionised water–ethanol mixture, repeatedly permitting the residue to decant under the influence of a magnet and while discarding the supernatant. Finally, the pure precipitate obtained was dried in a vacuum oven for 12 h at 60 °C.

2.3. Characterisation

Fourier transform infrared spectroscopy (FTIR), Thermo Scientific Nicolet iS10 (Thermo Fisher Scientific, Waltham, MA USA) (Smart iTR) with a diamond-based ATR compartment was used to determine the chemical molecular structure of the prepared CNC-MIONP adsorbent before and after adsorption together with its precursor materials. The spectral resolution was set to 4 cm^{-1} over 4000 and 500 cm^{-1} wavelength range.

Surface morphology was examined using a scanning electron microscope (JEOL-IT 7500LA, JEOL Ltd., Tokyo, Japan) with an accelerating 15–20 kV voltage.

Using the pH drift equilibrium approach, the pH of the point of zero charge (pH_{PZC}) for Fe_3O_4 and CNCs-Fe_3O_4 was obtained. Ten 250 mL flasks were filled to the brim with 50 mL volumes of the 0.01 M NaCl stock solution. By adding 0.1 M NaOH/HCl solution dropwise, the solutions' pH was adjusted between 1 and 12, giving each flask a unique pH value. A total of 0.1 g of Fe_3O_4 and CNCs-Fe_3O_4 were dispersed in several flasks with different pH levels. Before measuring the final pH, the solutions were allowed to equilibrate for 48 h. The pH_{PZC} of the prepared samples served as the intersection point.

2.4. Batch Adsorption Studies

Batch experiments investigated the impact of pH, initial pollutant concentration, adsorbent mass, contact time, and temperature on the adsorption of hexavalent chromium by CNCs-MIONPs. A 1000 mg/L Cr(VI) stock solution was prepared and diluted to the desired concentrations. The adsorbent removal efficiency was calculated using Equation (1), where Co represents the initial concentration and Ce indicates the end concentration in milligrams per litre (mg/L).

$$\% \text{ Removal of Cr(VI)} = ((\text{Co} - \text{Ce}))/\text{Co} \times 100\% \quad (1)$$

2.4.1. Effect of pH

To investigate how pH affects adsorption, dilutions of 100 mg/L from the stock solution were made in different 250 mL volumetric flasks. The pH of the solution in separate flasks was adjusted from 1.0 to 12.0 using 0.1 M HCl and 0.1 M NaOH, respectively. The CNC-MIONP adsorbent optimal mass (2.0 g) was added into a separate sealable flask simultaneously, containing 40 mL of the solution, and agitated for 90 min at room temperature using an automatic electric shaker.

2.4.2. Adsorbent Dosage

The effect of adsorbent dosage on the sorption studies was investigated experimentally by transferring 40 mL of 100 mg/L hexavalent chromium solution into 50 mL separate sealable bottles containing the adsorbent with masses ranging from 0.25 g to 2.0 g of the solutions, an automated electric shaker was used to maintain an agitation duration of 90 min at 250 rpm.

2.4.3. Hexavalent Chromium Concentration

Hexavalent chromium dilutions ranging from 0.5 mg/L to 100 mg/L were prepared in separate 250 mL volumetric flasks and set to the experimental optimum pH to evaluate how the adsorbate concentration affects adsorbent effectiveness. The 250 mL stock solution was divided into at least 40 mL of each solution, which was then put into a sealable container and agitated at room temperature with the ideal mass of the adsorbent and ideal adsorption time.

2.5. Adsorption Kinetics

The effect of time on the adsorption was explored by using optimum conditions from the above parameters with a time range between 30 s and 120 min, where 40 mL of the optimal concentration was transferred into sealable flasks containing the optimal mass of the adsorbent and then agitated at 250 rpm.

2.6. Spectrophotometric Analysis

After adsorption experiments, Cr(VI) concentrations were analysed spectrophotometrically using the Diphenyl Carbazide procedure at a wavelength of 540 nm [18].

3. Results and Discussions

3.1. Spectroscopic Analysis

The infrared spectra of CNCs-MIONPs reveal functional group changes (Figure 1). The broad peak at 3100–3500 cm^{-1} represents O-H stretching, while 2800–2950 cm^{-1} indicates C-H stretching. The peaks at 1600–1650 cm^{-1} are due to O-H bending from the absorbed water, and 1050 cm^{-1} shows C-O-C stretching. Cellulosic β-glycosidic linkages have been connected to the 900 cm^{-1} peak [19,20]. The CNC-MIONP spectrum shows reduced intensity at 3340 cm^{-1} due to Fe binding to O-H groups. The C-H bonds are seen at 2988 cm^{-1} and 2292 cm^{-1}. The Fe-O peaks at 554 cm^{-1} confirm nanoparticle incorporation, enhancing sorption sites by increasing oxygen-containing groups [21].

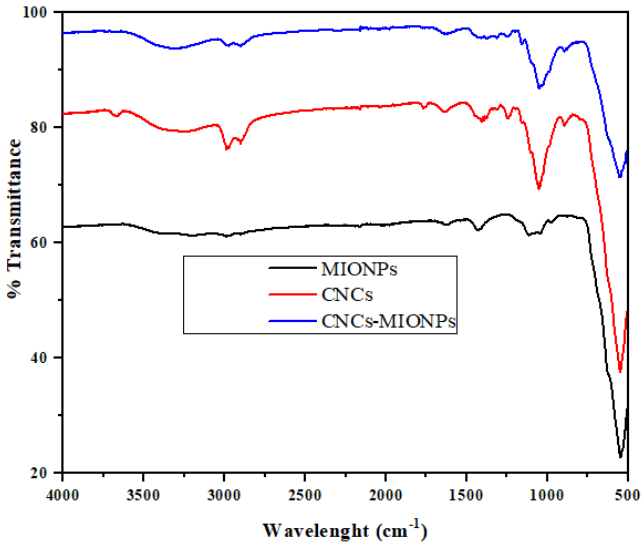

Figure 1. FTIR spectra for CNCs-MIONPs.

Scanning electron microscopy (SEM) images of CNCs-MIONPs before and after adsorption reveal significant surface changes (Figure 2). Before adsorption, the surface is coarse with visible pores and clumps, indicating effective adsorption sites. After adsorption, the surface became smooth, compact, and non-porous due to Cr(VI) adherence. The reduction in visible pores suggests these sites were occupied by hexavalent chromium, and the observed agglomerations are due to the attraction forces between the adsorbate and adsorbent.

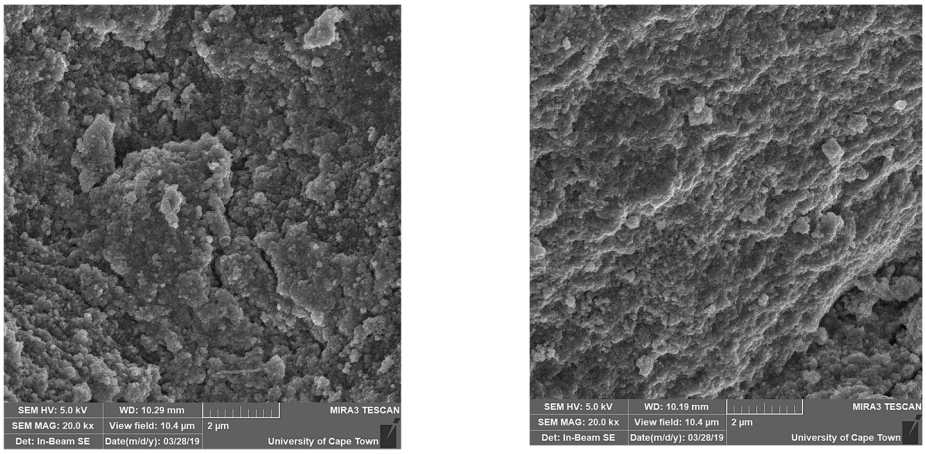

(**a**) (**b**)

Figure 2. SEM images of CNCs-MIONPs before adsorption (**a**) and CNCs-MIONPs after adsorption (**b**).

The isoelectric point (IEP) pH at zero-point charge (pHPZC) of the Fe_3O_4 was close to pH 6.7, while CNCs-Fe_3O_4 was 7.5 (Figure 3). Research studies indicate that when iron atoms coordinate with readily dissociable H_2O molecules, surfaces formed of Fe_3O_4 become hydroxyl functionalised. These hydroxyl groups on the amphoteric surface react with bases or acids to create a pH_{PZC} that is extremely near to neutral. The charge on Fe_3O_4 surfaces can be either positive or negative depending on the pH of the solution. The surface is protonated below the isoelectric point, generating $\equiv$ -$FeOH^{2+}$, resulting in a net positive charge. The surface hydroxyl groups are deprotonated to produce $\equiv$ -Fe-O^{-} surface groups above the isoelectric point [22]. The magnetic iron oxide nanoparticles are highly unstable because of their surface density charge (σ), which is too small in the IEP. The nanoparticles

may clump together and flocculate as a result. Studies from the literature indicate that the superficial charge must be altered using a variety of organic or inorganic surface modifiers to prevent agglomerations [23].

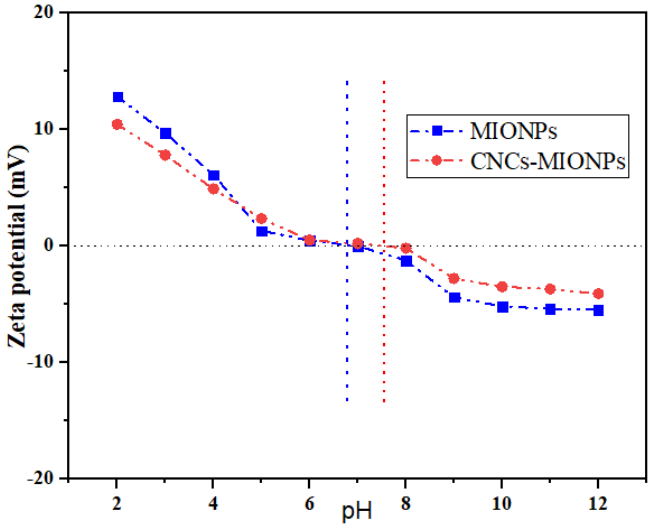

Figure 3. Zeta potential measurements.

3.2. Adsorption Studies

3.2.1. Effect of Solution pH on Hexavalent Chromium Sorption

The adsorption of hexavalent chromium by CNC-MIONP nanocomposite was significantly influenced by pH, as shown in Figure 4a. The highest adsorption efficiency, 90.23%, was recorded at pH 2.0, decreasing as the solution became more basic. Lie et al. (2020) established that in aqueous solutions with a pH range of 2.0–8.5, the bulk metal ions that exist are $M^{+/2+}$ or $M(OH)^{+}$ ions [24]. Most metal ions produce $M(OH)^{2+}$ above this pH (basic nature) of the solution, hence precipitating. Therefore, conducting adsorption experiments below pH 9.0 is always safe to prevent metal ion precipitation. Similarly, the concentration of H_3O^+ ions is substantially larger and exceeds that of metal ions at very low pH values. Excessive H_3O^+ ions cover the active sites of the adsorbent, allowing the metal ions to move about freely in the solution [25], translating to competing reactions between the adsorbate metal ion H_3O^+ ions. As the pH of the solution increases, there is less competition, and positively charged metal ions stick to available binding sites on the adsorbent [26].

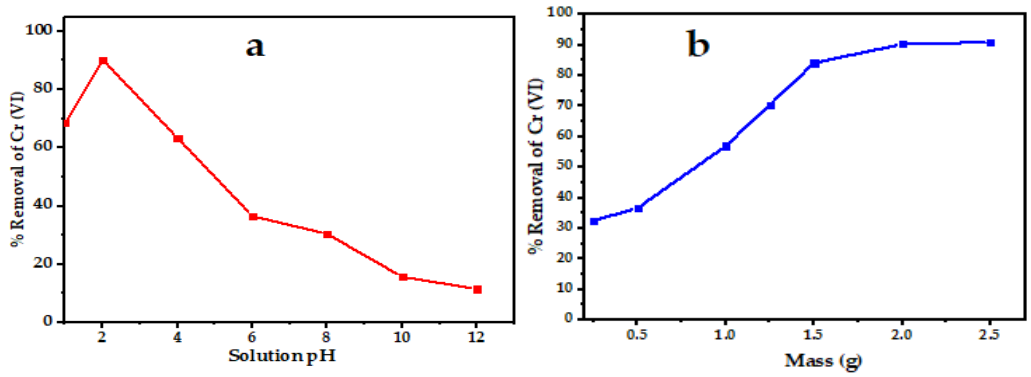

Figure 4. Effect of solution pH (**a**) and adsorbent mass (**b**).

Furthermore, pH_{PZC} is vital in increasing adsorption capacity at high solution pH, as the adsorbents showed pH_{PZC} values of 6.7 to 7.5. This pH dependency is attributed to the changes in surface charge, ionisation extent, and speciation of the nanocomposite. High

proton concentrations on the adsorbent surface at low pH enhance electrostatic interactions with chromate ions. Predominant chromium species at pH 1.0–6.0 include $Cr_3O_{10}^{2-}$, $HCrO_4^-$, $Cr_2O_7^-$, and $Cr_4O_{13}^{2-}$, with $HCrO_4^-$ being the most common. At higher pH values, the most predominant species are $Cr_2O_7^{2-}$ and CrO_4^{2-}, which create repulsive forces between the OH^- ions on the surface of the adsorbate and the negatively charged adsorbate. Furthermore, active site competition exists between CrO_4^{2-} and OH^- [27]. It is also evident that under acidic conditions, Cr(VI) is reduced to Cr(III) in the presence of an adsorbate, as depicted in Equation (2) below. In basic solutions, hexavalent chromium is less oxidised and exists as in Equation (3).

$$Cr_2O_7^{2-}{}_{(aq)} + 14H^+{}_{(aq)} + 6e^- \rightarrow 2Cr^{3+}{}_{(aq)} + 7H_2O_{(aq)}\ E^0 = 1.33\ V \quad (2)$$

$$Cr_2O_7^{2-}{}_{(aq)} + 4H_2O_{(l)} + 3e^- \rightarrow 5OH^-{}_{(aq)} + Cr(OH)_{3\,(aq)}\ E^0 = -0.13\ V \quad (3)$$

3.2.2. Effect of Adsorbent Dosage

This study examined the impact of adsorbent mass on Cr(VI) removal efficiency using a pollutant concentration of 0.5 mg/L for 90 min (Figure 4b). Using 40 mL of the Adsorbate, the absorption of chromium was increased from 32.58% to 90.31% by increasing the mass of the adsorbent from 0.25 g to 2.0 g. For 2.5 g, the uptake rate plateaued at 90.97%. This is explained by the fact that the entire adsorption system has a fixed number of possible adsorbent sites per unit mass of total adsorbent, and increasing the total mass of the adsorbent is likely to result in a reduction in the active sites per mass of the adsorbent, as well as a decrease in adsorption capacity. In addition, increasing the adsorbent dose reduces the solute concentration difference between the surface and bulk of the adsorbent [28]. Studies also reveal that the adsorbent particles interact with one another, and any system with excess solids may occasionally block potential active sites, resulting in a decreased adsorption capacity [29]. This is why 2.0 g was selected as the optimum dose of adsorbent.

3.2.3. Effect of Adsorbate Feed

The effect of starting hexavalent chromium ion concentrations was investigated at the different working concentrations of 5, 10, 20, 50, 75, and 100 mg/L. The other experimental variables were operated at predefined conditions set at a room temperature (298 K), pH of 2.0, shaking rate of 200 rpm, and adsorbent dosage of 1 g/L. The experiments were performed at a contact time of 150 min. Figure 5a shows the adsorption capacity profile plots at different adsorbate concentrations. The findings showed an enhanced adsorption capacity of 4.31 mg/g to 45.43 mg/g as the hexavalent chromium concentrations increased from 5 to 100 mg/L. The adsorbent removal rate was rapid within the first 30 min and sharply increased to around 90 min, then gradually stagnated after approaching equilibrium at 120 min. Studies show that the rapid sorption of the adsorbents must be due to the adsorbent's hydrophilicity, the conformational flexibility of various functional groups, larger surface area, and a more significant number of exchange sites, which are seen to decrease with time [30]. Since the adsorption kinetics rely on the surface area of the adsorbents, the initial higher rate might result from more sorption and binding sites being available on the adsorbents' surface. At the more reactive locations, metal ions were adsorbed. The adsorption process grows more complex, and the sorption process tends to be less favourable as these sites are gradually occupied. Studies in the literature further confirmed that the adsorption of metal ions portrays these general characteristics [31].

Furthermore, the concentration gradient rose with an increase in the initial metal ion concentration, which improved adsorption, but the mass transfer resistance decreased the removal efficiency [32]. The system's ability to remove metal ions is reduced since there is greater competition among the excess metal ions to adhere to an adsorbent surface. This can be justified by the decrease in the removal efficiency from 98.95% to 43.60% when the initial metal ion concentration is increased from 5 mg/L to 100 mg/L (Figure 5b). The decline is due to the saturation of active exchange sites on the adsorbent and increased competition

for these sites at higher initial concentrations. Higher concentrations provide a greater driving force for mass transfer, but as sites become occupied, adsorption efficiency drops.

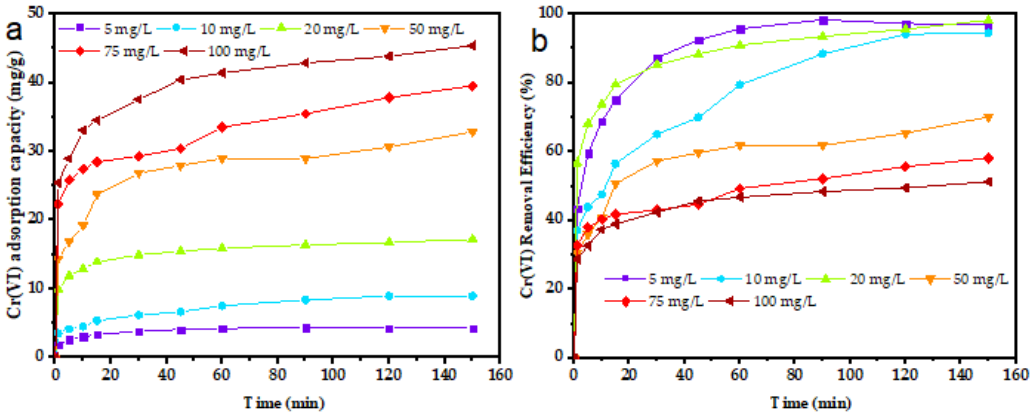

Figure 5. Effect of initial adsorbate concentration: (**a**) adsorption capacity; (**b**) adsorption efficiency.

3.3. Kinetics Studies

As shown in Table 1, the experimental results indicate that the sorption of Cr(VI) by CNCs-MIONPs initially fits a linear pattern but deviates over time. Kinetic experiments revealed that the pseudo-second-order kinetic model showed high correlation coefficients ($R^2 > 0.995$) compared to a pseudo-first-order model with R^2 less than 0.99, indicating it effectively describes the sorption process. The pseudo-second-order kinetic model suggests that chemical sorption, involving valence forces through electron sharing or exchange, is the dominant mechanism. The inter-particle diffusion results showed that boundary diffusion occurs first, followed by inter-particle diffusion. The findings suggested that diffusion through the thin layer around the adsorbent particles and inter-particle contact played critical roles in the sorption mechanism.

Table 1. Kinetic parameters.

Models	Kinetic Values				
	q_e (exp) (mg/g)	q_e (calc) (mg/g)	R^2	K_1	K_{id}
Pseudo-first order	76.34	0.69	0.9785	0.050	
Pseudo-second order	16.32	5.26	0.9999	0.1327	
Inter-particle diffusion model	18.32	10.89	0.9942		2.33

4. Conclusions

The current work effectively developed and characterised a CNC-MIONP nanocomposite adsorbent. The adsorbent demonstrated excellent Cr(VI) adsorption efficiency at an optimal pH of 2.0, an initial concentration of 0.5 mg/L, and a contact time of 90 min with a shaking rate of 250 rpm, achieving a removal efficiency of 91.78%. The increased surface area, smaller particle size, and the nanocomposite's active sites facilitated chromium species' immobilisation, enhancing chromate ion removal. The adsorption process involved chemisorption, where valence forces such as electron sharing or exchange occur between the adsorbate and sorbent. The pseudo-second-order kinetic model revealed that chemisorption was the rate-limiting mechanism. Thus, the nanocomposite presents a potential adsorbent for wastewater purifications.

Author Contributions: E.S. contributed to the synthesis, manuscript preparation, and communication. H.R. provided the chemicals, coordinated sample characterisation, and proofread the draft article. T.S. was engaged in the article development and data analysis. L.K. assisted in sample collection, setting up the experiments, characterisation, and proofreading the draft manuscript. W.O. helped set up experiments and proofread the draft article. All authors have read and agreed to the published version of the manuscript.

Funding: This research received no external funding.

Institutional Review Board Statement: Not applicable.

Informed Consent Statement: Not applicable.

Data Availability Statement: The data supporting this study's findings are available upon request from the corresponding author. The data are not publicly available due to privacy or ethical restrictions.

Acknowledgments: The authors thank the Department of Chemical Engineering and Chemistry, Vaal University of Technology, for providing the necessary laboratory space, chemicals, and equipment for the work's success and the University of Cape Town, South Africa, for SEM analysis.

Conflicts of Interest: The authors declare no conflicts of interest.

References

1. Ahmed, S.F.; Mofijur, M.; Nuzhat, S.; Chowdhury, A.T.; Rafa, N.; Uddin, M.A.; Inayat, A.; Mahlia, T.M.I.; Ong, H.C.; Chia, W.Y. Recent developments in physical, biological, chemical, and hybrid treatment techniques for removing emerging contaminants from wastewater. *J. Hazard. Mater.* **2021**, *416*, 125912. [CrossRef]
2. Organisation, W.H. International decade for action water for life, 2005–2015. *Wkly. Epidemiol. Rec. Relevé Épidémiologique Hebd.* **2005**, *80*, 195–200.
3. Salman, S.M. United Nations General Assembly Resolution: International decade for action, water for life, 2005–2015: A water forum contribution. *Water Int.* **2005**, *30*, 415–418. [CrossRef]
4. Turok-Squire, R.L. The Pressure of Incommensurability: When Water Is Life Becomes Water for Life at the United Nations. In *Globalisation, Ideology and Social Justice Discourses*; Springer: Berlin/Heidelberg, Germany, 2022; pp. 229–241.
5. Sharma, P.; Singh, S.P.; Parakh, S.K.; Tong, Y.W. Health hazards of hexavalent chromium (Cr (VI)) and its microbial reduction. *Bioengineered* **2022**, *13*, 4923–4938. [CrossRef]
6. Khan, Z.I.; Ahmad, K.; Siddique, S.; Ahmad, T.; Bashir, H.; Munir, M.; Mahpara, S.; Malik, I.S.; Wajid, K.; Ugulu, I. A study on the transfer of chromium from meadows to grazing livestock: An assessment of health risk. *Environ. Sci. Pollut. Res.* **2020**, *27*, 26694–26701. [CrossRef]
7. Mohod, C.V.; Dhote, J. Review of heavy metals in drinking water and their effect on human health. *Int. J. Innov. Res. Sci. Eng. Technol.* **2013**, *2*, 2992–2996.
8. Chai, W.S.; Cheun, J.Y.; Kumar, P.S.; Mubashir, M.; Majeed, Z.; Banat, F.; Ho, S.-H.; Show, P.L. A review on conventional and novel materials towards heavy metal adsorption in wastewater treatment application. *J. Clean. Prod.* **2021**, *296*, 126589. [CrossRef]
9. Rashid, R.; Shafiq, I.; Akhter, P.; Iqbal, M.J.; Hussain, M. A state-of-the-art review on wastewater treatment techniques: The effectiveness of adsorption method. *Environ. Sci. Pollut. Res.* **2021**, *28*, 9050–9066. [CrossRef]
10. Saleh, T.A.; Mustaqeem, M.; Khaled, M. Water treatment technologies in removing heavy metal ions from wastewater: A review. *Environ. Nanotechnol. Monit. Manag.* **2022**, *17*, 100617. [CrossRef]
11. Malik, S.; Muhammad, K.; Waheed, Y. Nanotechnology: A revolution in modern industry. *Molecules* **2023**, *28*, 661. [CrossRef]
12. Khan, I.; Saeed, K.; Khan, I. Nanoparticles: Properties, applications and toxicities. *Arab. J. Chem.* **2019**, *12*, 908–931. [CrossRef]
13. Ali, A.; Zafar, H.; Zia, M.; ul Haq, I.; Phull, A.R.; Ali, J.S.; Hussain, A. Synthesis, characterisation, applications, and challenges of iron oxide nanoparticles. *Nanotechnol. Sci. Appl.* **2016**, *9*, 49–67. [CrossRef]
14. Evans, S.K.; Wesley, O.N.; Koech, L.; Nelana, S.M.; Rutto, H.L. Structural Features of Cellulose and Cellulose Nanocrystals via In Situ Incorporation of Magnetic Iron Oxide Nanoparticles: Modification and Characterisation. *Coatings* **2022**, *13*, 39. [CrossRef]
15. Suter, E.K.; Rutto, H.L.; Wesley, O.N.; Banza, M. Stabilized Bare Superparamagnetic Iron Oxide Nanoparticles: Synthesis and Characterisation. *J. Nano Res.* **2023**, *80*, 81–96. [CrossRef]
16. Raj, V.; Chauhan, M.S.; Pal, S.L. Potential of sugarcane bagasse in remediation of heavy metals: A review. *Chemosphere* **2022**, *307*, 135825. [CrossRef]
17. Evans, S.K.; Wesley, O.N.; Nathan, O.; Moloto, M.J. Chemically purified cellulose and its nanocrystals from sugarcane baggase: Isolation and characterisation. *Heliyon* **2019**, *5*, e02635. [CrossRef]
18. Wiryawan, A.; Retnowati, R.; Burhan, P.; Syekhfani, S. Method of analysis for determination of the chromium (Cr) species in water samples by spectrophotometry with diphenylcarbazide. *J. Environ. Eng. Sustain. Technol.* **2018**, *5*, 37–46. [CrossRef]
19. Johar, N.; Ahmad, I.; Dufresne, A. Extraction, preparation and characterisation of cellulose fibres and nanocrystals from rice husk. *Ind. Crop. Prod.* **2012**, *37*, 93–99. [CrossRef]
20. Stuart, B.H. *Infrared Spectroscopy: Fundamentals and Applications*; John Wiley & Sons: Hoboken, NJ, USA, 2004.

21. Lin, S.; Xu, M.; Zhang, W.; Hua, X.; Lin, K. Quantitative effects of amination degree on the magnetic iron oxide nanoparticles (MIONPs) using as adsorbents to remove aqueous heavy metal ions. *J. Hazard. Mater.* **2017**, *335*, 47–55. [CrossRef]
22. Cristiano, E.; Hu, Y.-J.; Siegfried, M.; Kaplan, D.; Nitsche, H. A comparison of point of zero charge measurement methodology. *Clays Clay Miner.* **2011**, *59*, 107–115. [CrossRef]
23. Favela-Camacho, S.E.; Samaniego-Benítez, E.J.; Godínez-García, A.; Avilés-Arellano, L.M.; Pérez-Robles, J.F. How to decrease the agglomeration of magnetite nanoparticles and increase their stability using surface properties. *Colloids Surf. Physicochem. Eng. Asp.* **2019**, *574*, 29–35. [CrossRef]
24. Li, T.; Huang, X.; Wang, Q.; Yang, G. Adsorption of metal ions at kaolinite surfaces: Ion-specific effects, and impacts of charge source and hydroxide formation. *Appl. Clay Sci.* **2020**, *194*, 105706. [CrossRef]
25. Cruz-Lopes, L.P.; Macena, M.; Esteves, B.; Guiné, R.P.F. Ideal pH for the adsorption of metal ions Cr^{6+}, Ni^{2+}, Pb^{2+} in aqueous solution with different adsorbent materials. *Open Agric.* **2021**, *6*, 115–123. [CrossRef]
26. Dhumal, R.; Sadgir, P. Bioadsorbents for the removal of salt ions from saline water: A comprehensive review. *J. Eng. Appl. Sci.* **2023**, *70*, 80. [CrossRef]
27. Dvoynenko, O.; Lo, S.-L.; Chen, Y.-J.; Chen, G.W.; Tsai, H.-M.; Wang, Y.-L.; Wang, J.-K. Speciation analysis of Cr (VI) and Cr (III) in water with surface-enhanced Raman spectroscopy. *ACS Omega* **2021**, *6*, 2052–2059. [CrossRef]
28. McKinley, J.P.; Jenne, E.A. Experimental investigation and review of the "solids concentration" effect in adsorption studies. *Environ. Sci. Technol.* **1991**, *25*, 2082–2087. [CrossRef]
29. Qasem, N.A.; Mohammed, R.H.; Lawal, D.U. Removal of heavy metal ions from wastewater: A comprehensive and critical review. *NPJ Clean Water* **2021**, *4*, 36. [CrossRef]
30. Burtch, N.C.; Jasuja, H.; Walton, K.S. Water Stability and Adsorption in Metal–Organic Frameworks. *Chem. Rev.* **2014**, *114*, 10575–10612. [CrossRef]
31. Ugbea, F.A.; Ikudayisi-Ugbeb, V.A.; Yakubuc, M.O. Adsorptive removal of Cd^{2+}, Cr^{3+} and Cr^{6+} using natural and synthetic goethite particles: Kinetics study. *J. New Technol. Mater.* **2020**, *10*, 29. [CrossRef]
32. Rudi, N.N.; Muhamad, M.S.; Te Chuan, L.; Alipal, J.; Omar, S.; Hamidon, N.; Abdul Hamid, N.H.; Mohamed Sunar, N.; Ali, R.; Harun, H. Evolution of adsorption process for manganese removal in water via agricultural waste adsorbents. *Heliyon* **2020**, *6*, e05049. [CrossRef]